Lithography-based manufacturing of advanced ceramics for orthopaedic applications

Paterlini, Ambra; Stamboulis, Artemis; Turq, V; Laloo, Ryan; Schwentenwein, M; Brouczek, D; Piccinini, M; Bertrand, G

DOI:
10.1016/j.oceram.2021.100170

Open Ceramics 8 (2021) 100170

Contents lists available at ScienceDirect

Open Ceramics

journal homepage: www.sciencedirect.com/journal/open-ceramics

Lithography-based manufacturing of advanced ceramics for orthopaedic applications: A comparative tribological study

A. Paterlini [a,b,*], A. Stamboulis [a], V. Turq [c], R. Laloo [c], M. Schwentenwein [d], D. Brouczek [d], M. Piccinini [b], G. Bertrand [e]

[a] Biomaterials Research Group, School of Metallurgy and Materials, University of Birmingham, Edgbaston, Birmingham, B15 2SE, United Kingdom
[b] Lincotek Trento SpA, Italy
[c] CIRIMAT, Université de Toulouse, CNRS, Université Toulouse 3 – P. Sabatier, France
[d] LITHOZ GmbH, Austria
[e] CIRIMAT, Université de Toulouse, CNRS, INP-ENSIACET, France

ARTICLE INFO

Keywords:
Additive manufacturing
Zirconia-toughened alumina
Tribology

ABSTRACT

Ceramics long history in biomedical field is related to their high biocompatibility and mechanical properties. Precisely, for joint replacements, wear resistance is fundamental, so advanced ceramics as alumina and zirconia are preferred. Developments in ceramic additive manufacturing allow for dense ceramic parts with improved mechanical properties and shape accuracy.

This paper focuses on the tribological analysis of stereolithography-manufactured components for orthopaedics. Alumina, yttria-stabilised zirconia, 10 and 20 wt% zirconia toughened alumina (ZTA) samples were analysed. The effect of surface finishing, microstructure and microhardness on wear was considered.

Printing orientation does not significantly impact microhardness, wettability, and microporosity. However, some printing artefacts as the staircase effect were observed on spherical surfaces. Zirconia system presented high wear rates and friction coefficient, while alumina system showed more acceptable and stable values, with the formation of a self-mated tribofilm. ZTA composites presented the lowest wear volume and better mechanical and surface properties in general.

1. Introduction

In recent years, Additive Manufacturing (AM) of ceramics has received an increased interest in several areas, with particular attention to the medical field [1–4]. The stereolithography method consists of selectively UV curing photopolymerisable resins layer-by-layer to generate three-dimensional parts onto a platform that can either be immersed in a vat filled with slurry (top-down approach) or hung upside-down and approached by a thin coat of slurry when the layer is generated (bottom-up approach) [5–8]. A green part is created during this step, and a thermal treatment must follow to remove the polymeric component (debinding) and sinter the ceramic part. An appropriate thermal treatment cycle enables to sinter dense ceramic components with high mechanical properties. As a result, the range of stereolithography printable materials is increased compared to other AM technologies. Furthermore, the UV light source, either a micrometric laser (for laser stereolithography - SLA) or a digital mirror device (for digital light processing - DLP), allows the manufacturing of extremely accurate 3D parts, with a resolution in the order of 25 μm [1,9,10]. One of the advantages of AM for medical applications is the freeform design that facilitates the 3D printing of complex shapes and of porous, semi-porous or graded structures [1,11,12] beneficial for bone tissue repair and reconstruction [13–15].

Like most implantable components, orthopaedic implants must be biocompatible and exhibit mechanical properties such as wear resistance. For joint prostheses, implants generally include two parts continuously moving against each other. This specific function requires an evaluation of the tribological response of eligible materials. Tribology is a relatively recent discipline (its recognition started in 1966 [16]) that combines the analysis of friction, wear and lubrication of interacting surfaces in relative motion in a defined environment [17–19]. The study of tribological behaviour of orthopaedic implant

* Corresponding author. Biomaterials Research Group, School of Metallurgy and Materials, University of Birmingham, Edgbaston, Birmingham, B15 2SE, United Kingdom.
E-mail address: ambra.paterlini@lincotek.com (A. Paterlini).

https://doi.org/10.1016/j.oceram.2021.100170
Received 25 June 2021; Received in revised form 14 August 2021; Accepted 16 August 2021
Available online 27 August 2021

components is essential to ensure mechanical durability in a long-term friction exposure without generating and dispersing debris in the surrounding environment. Therefore, common material pairs for these applications present high wear resistance and low friction coefficients (μ). They include advanced ceramics (zirconia, alumina), metals (titanium, chrome alloys) or polymers (Ultra High Molecular Weight Polyethylene, UHMWPE) [20–22]. The main bearing couples are ceramic-on-ceramic (CoC), metal-on-metal (MoM) and ceramic or metal on UHMWPE (CoP or MoP). Their friction coefficient μ in dry conditions lies in the range of 0.40–0.50 for ceramic-on-ceramic [23,24], 0.40–0.45 for metal-on-metal [25] and 0.2–0.25 for metals with an UHMWPE counterpart [26]. The friction coefficient significantly decreases in simulated body fluid environments such as bovine or calf serum in the case of orthopaedic applications [27–29]. The μ values are in the range of 0.15–0.22 for CoC [30], 0.22–0.27 for MoM [22] and 0.05–0.1 for MoP or CoP [31,32]. Despite the lower friction coefficients of MoP or CoP systems, UHMWPE components present a high wear debris volume that could generate serious health complications [33,34]. Thus, ceramic materials remain a valid alternative for load-bearing components, and additive manufacturing can be an efficient tool for the production of arthroplasty implants. However, there are limited studies about the tribology of AM parts [35–38], and even fewer about additive manufactured ceramic parts [39,40].

This paper focuses on the tribological study of the most common materials for arthroplasty implants: alumina, zirconia, and zirconia toughened alumina with different toughening percentages manufactured by digital light processing stereolithography. The primary purpose was to evaluate the use of AM technology for the production of joint implant components. Initial surface analyses, including surface profilometry, microporosity, and hardness, were carried out on the as-printed parts. The wettability was also measured by contact angle. After the tribological tests in wet and dry conditions, the surface evolution was tracked by white-light profilometry, as well as wear volume measurements. The microstructure of the tribofilm formed in the contact area was also studied.

2. Materials and methods

2.1. AM technology and materials

The CeraFab 7500 by Lithoz GmbH (Vienna, Austria), the predecessor of the CeraFab Lab currently available on the market, was selected for the manufacture of ceramic parts. This system is based on DLP printing with a bottom-up approach. The building platform dimensions are 76 × 43 mm^2 (X, Y). The LED light source for the polymerisation is integrated with a Digital Mirror Device (DMD) projector which has a lateral resolution of 1920 × 1080 (X, Y) pixels. The pixel size of 40 × 40 μm^2, corresponds to the smallest achievable detail. The *LithaLox 350* (98 vol%-pure α-alumina (A)) and *LithaCon 3Y 230* (3 mol % yttria stabilised zirconia (3YZ)) slurries supplied by Lithoz GmbH were used. In addition, two Lithoz GmbH under-development slurries of 10 and 20 wt% zirconia toughened alumina (ZTA10 and ZTA20, respectively) were implemented. Slurries consist of photocurable ceramic suspensions in which the ceramic powder is homogenously distributed. The organic components of the matrix are based on acrylates and methacrylates and the solid ceramic load was in the range of 45–50 vol%.

Fig. 1 presents the geometry and orientation regarding the printing direction for all samples: disc and ball for tribology and surface roughness and flat oriented cuboids for all other tests (microhardness, wettability, porosity and grain analysis). Oriented samples allowed for the evaluation of the printing direction effect (z-axis) on the different material properties.

Once printed, the green parts were cleaned with LithaSol 20 commercial solvent (by Lithoz GmbH) and pressurised air. After a drying step of 120 h at 100 °C to remove possible volatile additives from the

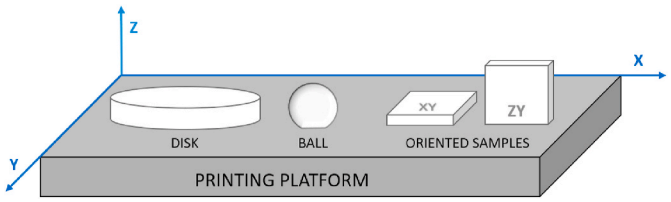

Fig. 1. Printed samples geometry and orientation.

printed component, debinding and sintering steps were performed at different temperatures depending on the materials. During the alumina and ZTA10 debinding, the temperature was increased by a 6 °C/h slow ramp until 400 °C and then 60 °C/h until 1100 °C. Sintering was performed with an average ramp of 60 °C/h until 1700 °C and 1650 °C for alumina and ZTA10 respectively; a dwell time of 2 h at maximum temperature was set in both cases. Thermal processes took 102 h for debinding and 48 h for sintering. For zirconia debinding, temperature was increased by averagely 12 °C/h until 350 °C; for sintering an average ramp of100 °C/h was used until 1450 °C. ZTA20 debinding was performed with an average ramp of 9 °C/h until 430 °C and followed by a faster average 100 °C/h ramp for sintering until 1550 °C. The entire thermal process of 3YZ and ZTA20 took 74 and 111 h respectively, with a dwell time of 2 h at sintering temperature in both cases.

2.2. Porosity measurements based on the Archimedes' principle

The Archimedes' test was carried out to measure the samples density ρ that was compared with the theoretical density ρ_T, provided by the supplier and confirmed through X-ray diffraction, of 4.01, 6.09, 4.13 and 4.34 g/cm^3 respectively for A, 3YZ, ZTA10 and ZTA20. The closed porosity $p = 1 - \rho/\rho_T$ was then calculated. The sample was first weighed in air and then in water. Given the water density ρ_0 (0.9986 g/cm^3 at 18 °C), ρ is calculated using Equation (1):

$$\rho = \frac{A}{A-B} \cdot (\rho_0 - \rho_a) + \rho_a \quad (1)$$

where ρ_a is the air density (0.0012 g/cm^3) and A and B the sample weight respectively in air and water.

2.3. White light interferometry

Surface profiles were analysed by an *S*-neox3D Optical Profiler (SENSOFAR®) by confocal scanning. The surface topography was collected using ×10 or ×20 magnification, while the focus range varied along the z-direction from −50 μm to +50 μm (with 0 corresponding to the focused sample surface) for flat surfaces (discs and oriented samples) and from −250 μm to +250 μm for ball surfaces. The roughness was measured using the S_a arithmetical mean height, which is defined as Equation (2), where μ is the arithmetical mean of the surface and z is the height of the measured point in the coordinates x and y [41,42].

$$S_a = \frac{1}{MN} \sum_{j=1}^{M} \sum_{i=1}^{N} \left| z(x_i, y_j) - \mu \right| \quad (2)$$

The scan covered a 1.3 mm × 1.75 mm area, with a lateral resolution of 1.3 μm/pixel. On discs, the roughness was measured on the top surface (xy-plane), on oriented samples, the roughness was measured on the lateral surface (xz- or yz-plane), while on balls, the roughness was measured by tilting the sample by 45° from the xy-plane, to analyse the same zone selected for tribology (as explained in paragraph 2.6). An average of 3 scans for 3 samples of each material were recorded and analysed.

2.4. Microindentations

The microhardness was measured by Vickers hardness, using a Buehler MicroMet 6000 hardness tester and the related DiaMet software. After a preliminary study, a 50 gf load was selected to perform the tests. The Vickers indenter is a pyramid-shaped diamond of 136° angle. Equation (3) gives the Vickers hardness HV which is the ratio between the applied load F_{kg} [kg_f] and the real contact area A_c [mm^2].

$$HV\left[\frac{kgf}{mm^2}\right] = \frac{F_{kg}}{A_c} = \frac{F_{kg}}{A_p}\cdot sin68^\circ = \frac{2\cdot F_{kg}}{D^2}\cdot sin68^\circ \quad (3)$$

where A_p is the projected area and D the average indentation diagonal. The DiaMet software was used to calculate the HV after optically measuring the length of the diagonals on the indentation. In average, 10 to 12 indentations were performed on each sample.

2.5. Wettability

The static contact-angle was measured on oriented samples (Fig. 1) using a Digidrop MCATV6 Gbx instrument. A 0.03 ml bovine serum droplet was manually deposited on the surface by a graduated syringe, and the related software allowed for the measurement of the contact angle through a magnifier camera. The test was performed for both printing direction surfaces, using discs and oriented samples; 5–6 serum droplets were generated for each sample, and 10 to 15 angle measurements were registered for each droplet. Before the analysis, a cleaning protocol was performed on all samples consisting of 5 min immersion in an ethanol ultrasonic bath, 10 min of drying at 70 °C and 20 min of cooling at room temperature. A preliminary analysis was also carried out to evaluate the spreading time of the droplet by measuring the contact angle variation over a period of time at regular intervals. This allowed establishing the correct range of time to perform the measurements by avoiding errors due to initial oscillations or later drop evaporation.

2.6. Tribology and wear volume analysis

The tribological behaviour of different materials was studied using a ball-on-disc CSEM tribometer, with a linear motion adaptor allowing to also perform reciprocating linear tests. Each couple of identical materials (ball and disc chosen of same nature) was tested 3 to 5 times to evaluate the repeatability and standard deviation of wear and friction coefficient. 20 mm of diameter and 3 mm thick discs were printed with the flat surface on the xy-plane, while the 10 mm diameter balls, illustrated in Fig. 2, were printed standing along the z direction (with the flat base on the xy-plane).

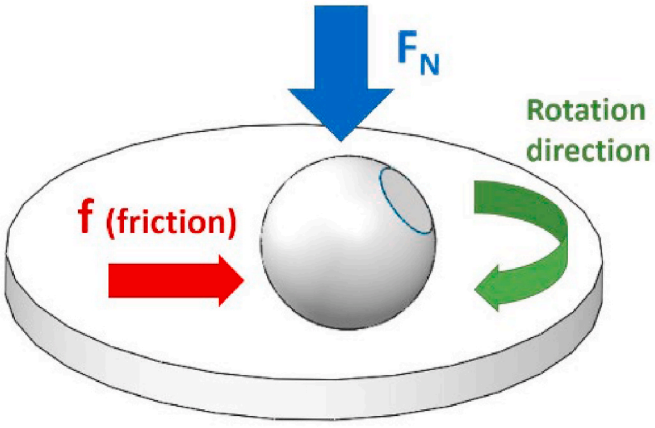

Fig. 2. Schematic view of the forces acting during the tribological test.

During rotary tests, the ball was stationary and loaded with a 5 N normal force L. The average theoretical Hertzian contact pressure was calculated according to Equation (4), where d is the diameter of the ball, E and ν the elastic modulus and Poisson's ratio of the material. E, ν values used were 220 MPa, 0.3 for zirconia and 340–360 MPa, 0.23 for alumina and ZTA (E values were obtained by microindentations and ν from literature [43–45]). The resulting contact pressure was 550 MPa for zirconia/zirconia and about 750 MPa for alumina/alumina and ZTA/ZTA.

$$P_{mean} = \frac{\sqrt[3]{L}}{\pi}\left[\frac{3d(1-\nu^2)}{4E}\right]^{-\frac{2}{3}} \quad (4)$$

The disc rotation speed was 3–9 cm/s on a circular pattern of 3–9 mm diameter for a total length of 50 m and a duration of around 30 min. Diameters were varied to optimise the number of disc samples used and the speed was adapted to the sliding length to maintain constant *laps per second* ratio, in order to obtain comparable wear data. Thanks to a force sensor measuring the deflection of the ball holder during sliding, this instrument allowed for the calculation of the friction coefficient $\mu = f/F_n$, where f is the tangential friction force and F_n the normal force corresponding to the 5 N load (Fig. 2).

A pin holder allowed fixing the ball at a tilt of 45° from the xy-plane (printing platform plane). This angle was chosen to represent a non-ideal scenario in terms of surface defects due to the staircase effect related to AM. As illustrated in Fig. 3, this effect can be related to pixels imaging during DLP polymerisation and layer slicing along z-axis. Tests were performed at room temperature in dry conditions and also in a lubricated environment to evaluate the tribological behaviour in wet conditions similar to those encountered *in vivo*. A Sigma-Aldrich bovine calf serum (ref. 12133C) diluted in distilled water at 50 vol% was used to obtain the recommended protein concentration of 30 g/l suggested by the ISO 14242 standard [28].

Linear reciprocating tribo-tests were also performed, with a 4 mm track length, during 50 000 cycles (around 9 h duration); speed and load were maintained at 2 cm/s and 5 N, respectively, in order to evaluate the long-term behaviour of the systems. The volume of wear debris generated by the tribological tests was measured thanks to the surface analysis of the profilometry cartographies using the SensoMAP 7.1 software. Some preliminary corrections were applied: an algorithm allowed for removing filling and non-measured points, and for a shape correction to obtain flat surfaces. Concerning the shape correction, a sphere was selected for ball surfaces, while a 3rd degree polynomial resulted in being the most appropriate approximation of the uneven discs' surface. After these corrections, the wear volume was measured using the 'hole analysis' method by manually circumscribing the worn zone on ball and disc counterparts, and adding the wear of both counterparts to obtain a total wear volume. The wear volume comparison was achieved through the Archard law [46], often used to describe the tribological behaviour of ceramics: K = VH/Fl [23,47,48], where K is a dimensionless constant that represents the wear coefficient, V is the sphere wear volume measured in mm^3, H [GPa] is the hardness, F [N] is the applied normal load, and l [m] is the total sliding length covered by the sphere during the test. Another important parameter is the specific wear rate k_S, defined as the ratio K/H or V/Fl ($mm^3 \cdot N/m$) and obtained by the Archard law. The wear coefficient and specific wear rate were calculated after the 50 000 cycles test (400 m). Examples of the two tracks topography on zirconia samples are shown in Fig. 4.

2.7. Microstructure analysis

The samples microstructure was analysed using an FEI Quanta450 SEM. A conducting coating was not required on those samples because low vacuum imaging mode and secondary electrons detection were used. The pressure was set in the range of 90–110 Pa, the voltage was between 10 and 12 kV, and the current was between 140 and 165 pA. In

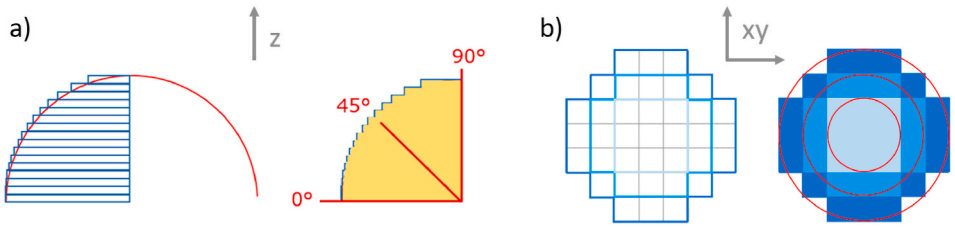

Fig. 3. Staircase effect approximations on a spherical surface due to a) slicing and b) pixels.

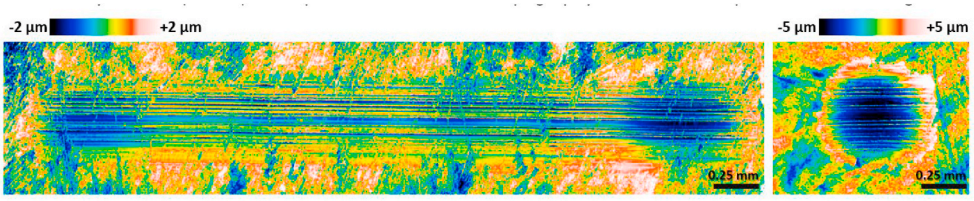

Fig. 4. Disc and ball tribology scars on zirconia samples.

the case of zirconia sintered parts, the protocol was changed to a high vacuum mode with decelerated back-scattered electrons detection, using a voltage of 1.5–4 kV and a current in the order of 1 pA. After the tribological tests, the samples were prepared by cross-section polishing using a JEOL IB-19510CP polisher. The ion-beam cut allowed for a polished cross-section without altering the surface. SEM images at ×2500 and ×5000 magnifications were also used for grain size analysis by ImageJ. After the scale setting (30 or 60 pixels/µm for ×2500 and ×5000 magnifications, respectively), the area of the grain was contoured using the *Freehand Selection* tool and measured by the *Analyse-Measure* tool. In ZTA10 and ZTA20 images, the contrast of zirconia grains was high enough to isolate them through a threshold. The binary image was then analysed using the *Analyse Particles* tool that allowed for measuring all grain areas. An average of 3 images and 15 grains for each image were analysed for every material.

3. Results

3.1. Roughness, porosity and grain size analysis

The roughness of balls and flat samples measured by white light interferometry is presented in Fig. 5a. Fig. 5b is an example of a ZTA20 ball surface showing the AM staircase effect, in this case due to DLP pixels (the steps direction opposes the printing layers). The two surface profiles indicate that on the one hand, the measured roughness of the sphere is directly related to the manufacturing steps (blue arrow and profile): both values in the order of 3 µm and steps dimensions are multiple of pixel areas (40 × 40 µm^2). On the other hand, the red profile measured along the step – by avoiding the waviness effect – recalls the xz-plane flat surface roughness in the order of 1 µm, and the printing layers (25 µm) are slightly visible as well. Zirconia and ZTA20 balls present the most irregular surfaces and the higher influence of AM approximations; for alumina and ZTA10 balls roughness is comparable with the xz-plane surface one. Generally, xy-plane flat samples showed significantly low roughness due to their laying printing direction (with the main surface parallel to the support platform), while the higher values encountered for xz-plane are affected by the printing layers.

The porosity values were very similar for all samples except for alumina, which presented a slightly higher porosity percentage. Alumina also presented larger grains compared to other materials. Zirconia and ZTA20 exhibited the smallest grain sizes. The data are shown in Table 1, for ZTA10 and ZTA20 average grain size was given for the two different grain populations: alumina (a*) and zirconia (z*).

3.2. Microindentations

The hardness values, expressed in GPa and HV, for both printing orientation (xz and xy) surfaces are presented in Table 2. There was no

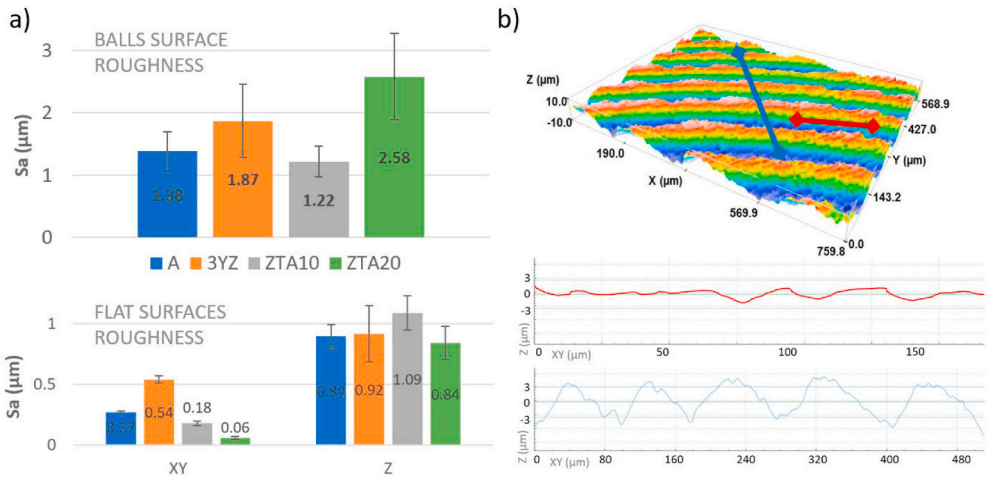

Fig. 5. (a) Spheres and flat surfaces roughness; (b) example of ZTA20 ball profilometry.

Table 1
Porosity and grain sizes of printed materials with a* = alumina grain size and z* = zirconia grain size.

Material	A	3YZ	ZTA10	ZTA20
Porosity (%)	1.83 ± 0.81	0.45 ± 0.27	0.67 ± 0.42	0.30 ± 0.27
Grain average diameter (μm)	6.15 ± 1.92	0.40 ± 0.14	a*: 1.85 ± 0.43 z*: 1.15 ± 0.27	a*: 0.83 ± 0.22 z*: 0.44 ± 0.08

Table 2
Hardness measured by microindentations on different printing orientation surfaces.

Material	A	3YZ	ZTA10	ZTA20
xy-plane hardness (GPa)	14.3 ± 1.8	12.0 ± 0.7	15.9 ± 1.2	16.6 ± 0.7
xz-plane hardness (GPa)	15.5 ± 1.6	12.0 ± 0.4	16.0 ± 0.8	17.4 ± 0.5
xy-plane hardness (HV)	1454 ± 170	1219 ± 60	1625 ± 110	1693 ± 70
xz-plane hardness (HV)	1584 ± 150	1227 ± 40	1631 ± 80	1774 ± 50

evidence of printing directions influence since, for each material, the hardness values on xy and xz surfaces were comparable.

3.3. Wettability

Fig. 6a shows the contact angle measurements to determine the surface wettability. An image of a diluted bovine serum droplet on the zirconia surface is shown in Fig. 6b. Xz-plane surface values of the contact angle are very similar, all in the range of 45°–50°, while the angles measured along xy-plane are more heterogeneous and varied from a minimum of 38° for alumina to a maximum of 61° for ZTA10.

3.4. Tribology and wear volume analysis

The frictional behaviour in "dry" (ambient air with a Relative Humidity range from 33 to 56%RH) and wet conditions (immerged in bovine calf serum) of the four sets of samples were investigated and compared with ball-on-disc rotary tribotests. Fig. 7 and Fig. 8 present the friction coefficient change as a function of the sliding distance during the rotational tribology test in dry and wet conditions, respectively. The dry tests presented a variety of initial friction coefficients for the four sets of samples; 0.15 for 3YZ/3YZ and ZTA20/ZTA20, 0.28 for ZTA10/ZTA10 and 0.5 for A/A. The change of the friction coefficient with the sliding distance was similar for alumina and ZTA systems, while zirconia 3YZ system showed a different trend. The friction coefficients for alumina/alumina and ZTA10/ZTA10 increased quickly to a value higher than 0.55 and reached a plateau after less than 10 m sliding. The ZTA20/ZTA20 coefficient increased more slowly for a distance of about 20 m, but stabilised at a plateau of approximately 0.5. On the other hand, the 3YZ/3YZ friction coefficient increased slowly and continuously without

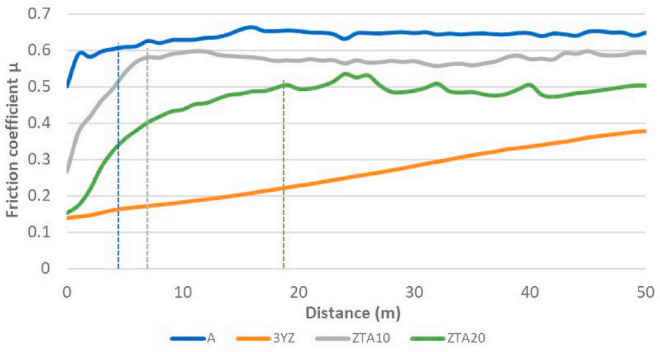

Fig. 7. Friction coefficient evolution for A/A, 3YZ/3YZ, ZTA10/ZTA10 and ZTA20/ZTA20 systems during 50 m-rotary tests in "dry" conditions (ambient air). Vertical dashed lines indicate the stabilization distance of the friction coefficient for the different systems.

reaching a plateau during the 50 m test. The tribological behaviour of the material samples in wet conditions was not very different among the set of samples tested; all sets of samples presented friction coefficient values between 0.15 and 0.25 at the end of the 50 m test, corresponding to more than a 50% reduction compared to the final dry condition values.

Concerning the long-term evolution of the frictional behaviour, Table 3 reports, for all sets of materials, the average final stable friction coefficients after 50 000 cycles (namely 400 m) linear reciprocating tests in "dry" conditions – calculated as the average μ for the last 100 cycles of the test – with the corresponding specific wear rate and wear coefficient.

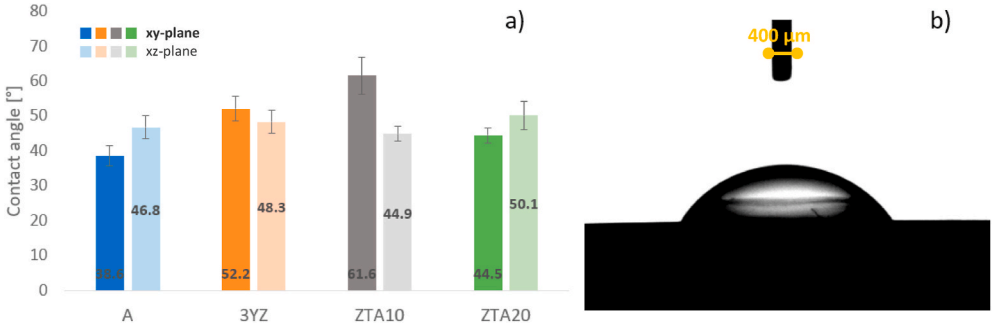

Fig. 6. (a) contact angles measured on xy-plane and xz-plane surfaces; (b) image of serum drop on 3YZ surface.

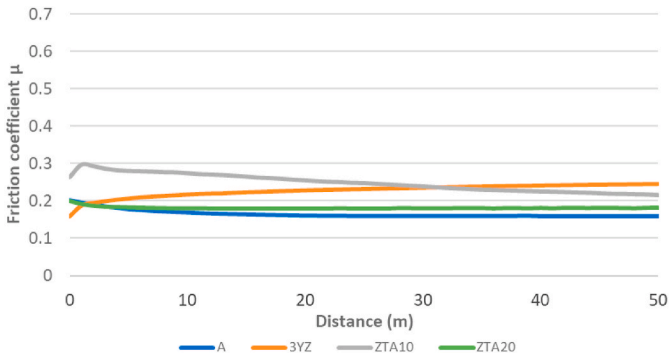

Fig. 8. Friction coefficient evolution for A/A, 3YZ/3YZ, ZTA10/ZTA10 and ZTA20/ZTA20 systems during 50 m-rotary tests in wet conditions (immersion in bovine calf serum).

The 3YZ/3YZ system presented the highest k_S and K values and a larger friction coefficient, while ZTA10/ZTA10 and ZTA20/ZTA20 exhibited a lower total wear volume despite having comparable friction coefficient to alumina. Concerning the friction coefficient values, some differences were noticed between the final values after the "dry" conditions longer linear reciprocating tests (400 m, Table 3) and the shorter rotary tests (50 m, Fig. 7). Thus, a detailed analysis of the wear and friction coefficient change with the sliding distance at 1 m, 50 m and 400 m during linear reciprocating tests was performed (Fig. 9 – detailed curves not shown). The A/A and both ZTA/ZTA systems exhibited similar behaviour regarding the wear volume variations, even if the A/A system exhibited a slightly higher wear rate than ZTA/ZTA. For the three sets of material samples, the wear volume variations in the selected range of the sliding distance were well fitted by a logarithmic trend. The friction coefficient was approximately constant for A/A, slightly increased for ZTA10/ZTA10 and more distinctly increased for ZTA20/ZTA20. On the other hand, 3YZ/3YZ showed a net linear increase for both wear and friction coefficients. The good correlation coefficients (0.99 and 1.00 for 3YZ and ZTA20, respectively) indicated a satisfactory fit for all samples.

3.5. Surface and cross-section microstructure evolution after wear

The microstructure of the wear surface of all samples before and after 50 000 cycles of linear reciprocating tribological test was studied by SEM to determine the long-term effect of friction on the surfaces and is presented in Fig. 10. For ZTA10 and ZTA20, there were no visible changes concerning the microstructure and the grain size (white grains were attributed to alumina and grey grains to zirconia), while 3YZ presented slightly deformed grains after tribology. The most noticeable transformation was found on the alumina sample where the micrograph of the wear surface shown in Fig. 10 suggested the formation of a tribofilm on the surface. The tribofilm was particularly evident in the pores and irregularities of the surface, which characterised the alumina samples (as in Table 1). Furthermore, the cross-section polishing preparation (Fig. 11) allowed for the estimation of the film thickness around 1–2 μm and the analysis of its microstructure. Grains in the tribofilm are significantly smaller comparing to alumina initial grains, and thin pores are detected at the interface between the film and the substrate. On the other hand, the cross-section of ZTA10 (Fig. 12) did not show any evidence of a tribofilm formation on the surface; the debris generated during friction only seemed to fill the few thin superficial cavities, resulting in a smoother final surface.

4. Discussion

Additive manufacturing has a significant impact on the surface finish, especially on irregular or non-flat surfaces such as spherical ones. As shown by profilometry analysis in Fig. 5a, there are three main surfaces to analyse: the xy and xz-oriented flat surfaces and the ball curved surface. Roughness variations along oriented flat surfaces are mainly related to printing layer orientations, while the ball roughness is strictly related to the staircase effect. The highest values were found for spherical curved surfaces, corresponding to the 'steps' (Fig. 5b). The smoothest surfaces were related to the xy-plane, and intermediate roughness values were measured along the xz-plane. As mentioned in paragraph 3.1, the staircase effect was particularly marked in the cases of ZTA20 and 3YZ, which presented ball roughness twice as high as the z-axis roughness or more. On the contrary, alumina and ZTA10 roughness values were comparable on the curved surface of the ball and z-axis, meaning a limited effect of the printing process.

All hardness values were in agreement with previous hardness studies in the literature (around 17 GPa for alumina, 13 for zirconia and in the range of 13–17 GPa for ZTA composites [49–52]), and according to Table 2, there were no significant differences between both printing orientations. Being the diagonal of indentations in the order of 7–9 μm almost half the size of the printing layer (25 μm height), statistically the presence of eventual interlayer defects would have been detected on the xz-plane. Thus, in terms of microhardness, the AM process did not

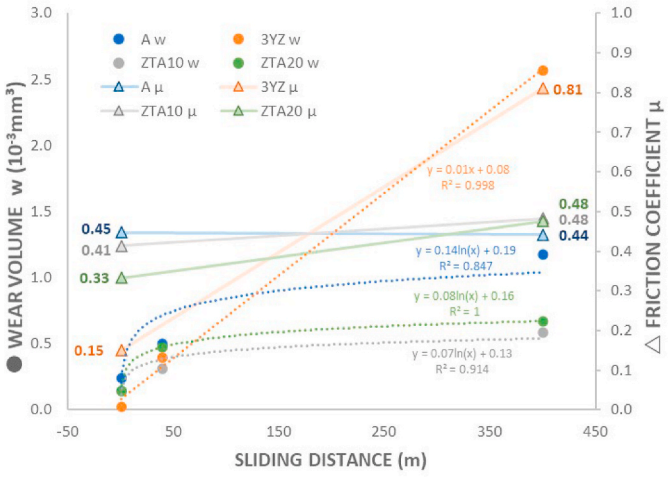

Fig. 9. Comparison of wear volume and friction coefficient as a function of the sliding distance for 1 m, 50 m and 400 m-linear reciprocating tests.

Table 3
– *Friction (μ), wear coefficient (K) and specific wear rate (k_S) after 50 000 cycles linear reciprocating test.*

Couple of materials	A/A	3YZ/3YZ	ZTA10/ZTA10	ZTA20/ZTA20
Final friction coefficient μ	0.44 ± 0.09	0.82 ± 0.09	0.48 ± 0.11	0.48 ± 0.11
Total wear volume (10^{-6} μm³)	1.17 ± 0.38	2.56 ± 0.68	0.58 ± 0.35	0.67 ± 0.15
Ball wear volume (10^{-6} μm³)	0.36 ± 0.12	1.03 ± 0.37	0.23 ± 0.08	0.24 ± 0.15
Wear rate k_S [10^{-8} N·mm³/m]	11.6 ± 4.05	33.4 ± 12.2	7.55 ± 2.67	7.83 ± 5.05
Wear coefficient K [10^{-7}]	17.3 ± 6.03	40.1 ± 14.6	13.1 ± 4.26	13.3 ± 8.58

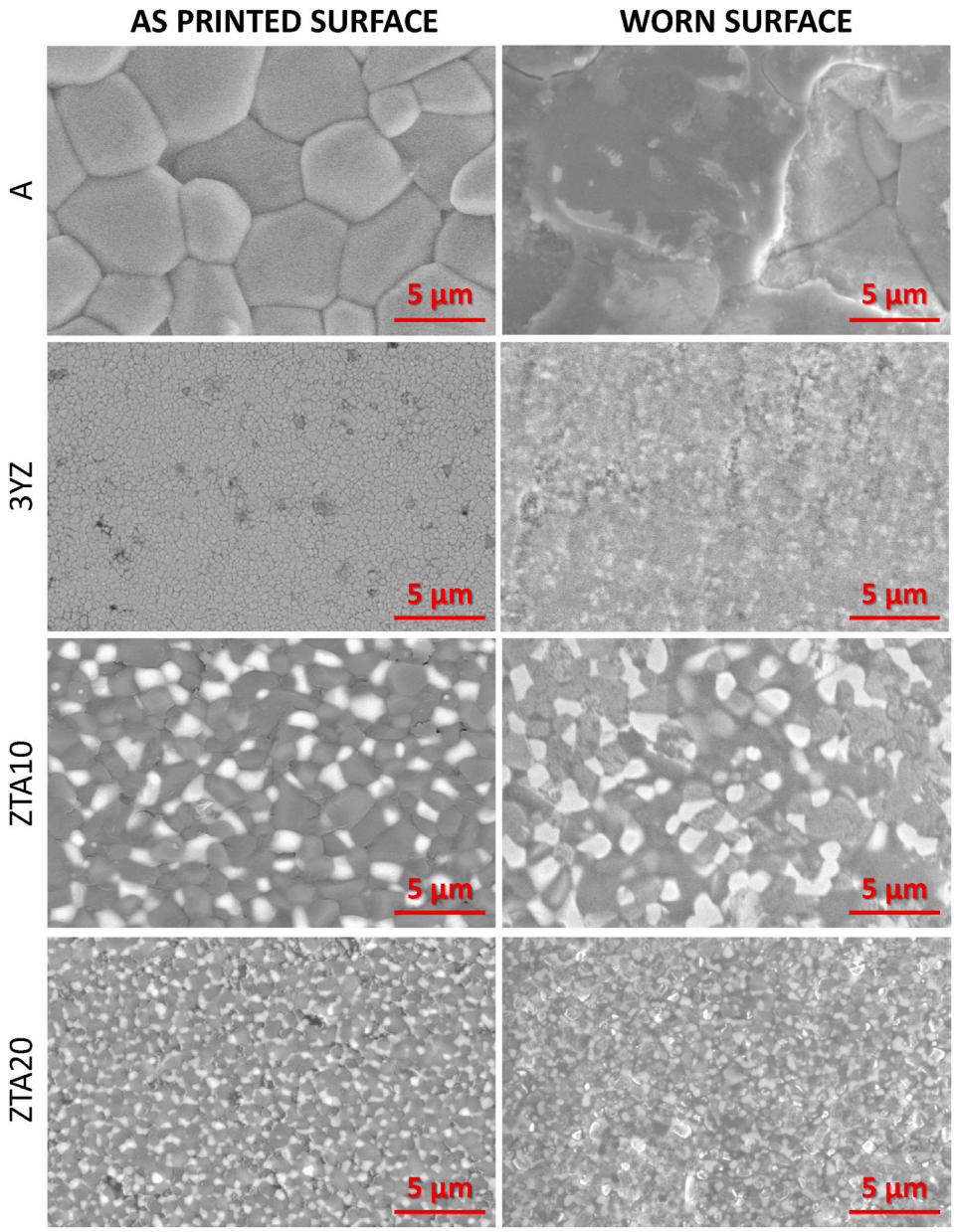

Fig. 10. Comparison of the microstructure of sample surfaces before and after 50 000 cycles.

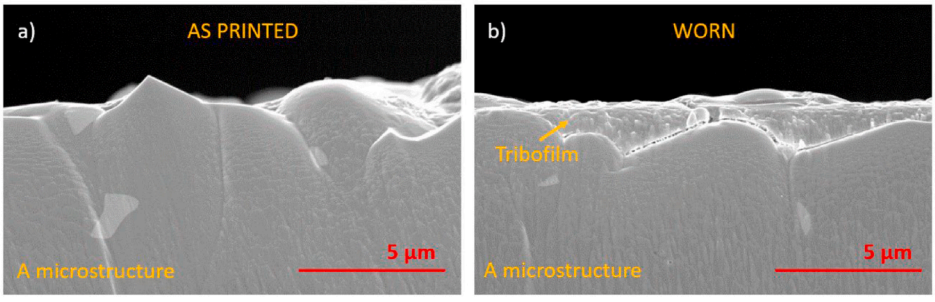

Fig. 11. Disc cross-section after alumina-on-alumina (A/A) 50 000 cycles tribotest: a) as printed unworn zone and b) worn surface and tribofilm.

impact the mechanical response of the four materials. Vickers micro-hardness measurements of ZTA compositions, both ZTA10 and ZTA20, were higher compared to pure alumina.

The contact angle measurements (Fig. 6) showed values lower than 90° for all samples, suggesting that all surfaces are hydrophilic and present interaction with the bovine serum probably due to the high surface energy. Similar contact angles were found for the four materials, in agreement with literature [53], when measurements are performed

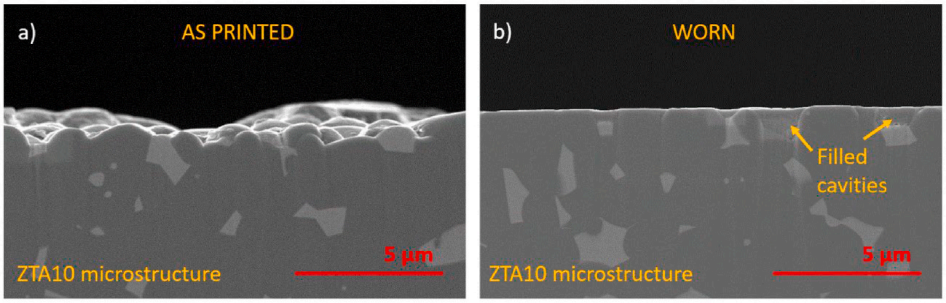

Fig. 12. Disc cross-section after ZTA10-on-ZTA10 (ZTA10/ZTA10) 50 000 cycles tribotest: a) as printed unworn zone and b) worn surface.

on z-oriented samples. Instead, measurements made on xy-plane surfaces exhibit differences among the different materials. An important parameter that controls wettability is roughness, the homogeneity of contact angles for xz-plane samples could be related to their high S_a roughness, in the order of 1 µm for all materials. However, wettability and roughness have not a linear relationship as reported in the literature [54]. This may explain the heterogeneity of xy-oriented samples. The presence of open porosity could also influence alumina low contact angle: with the penetration of bovine serum into the pores, the drop would spread more easily on the surface. The effect of the alumina wettability was also noticed in the wet tribological test results (Fig. 8), since this material presented significant differences between dry and wet condition friction coefficients. Large grains could create small tanks at the surface where the serum could be accumulated during the test, a phenomenon that is known to reduce friction [55]. Contrarily, ZTA10 discs (xy-oriented) presented the lowest wettability, and this could explain the higher initial friction coefficient during the lubricated test.

The effect of hardness on the wear has also been confirmed, in good agreement with the Archard law [46] for abrasive wear: harder material couples, such as alumina and ZTA compositions present lower wear rates (with similar friction coefficients), while lower hardness values coincide with higher wear as for zirconia. All wear rates, k_S, are in the order of 10^{-6} mm^3 N/m. This value is generally considered as the upper limit of mild wear behaviour for hard ceramics; higher rates between 10^{-6} and 10^{-4} mm^3 N/m were found to present a transition point from mild to severe wear according to load and sliding distance [23,56–58]. However, measured wear rates and coefficients are very similar to conventionally processed ceramic values according to state of the art: in the range of $5{\cdot}10^{-6} - 5{\cdot}10^{-5}$ mm^3 N/m and $10^{-5} - 5{\cdot}10^{-4}$ respectively [48,59,60].

The same can be noticed for friction coefficients: experimental values shown in Figs. 7 and 8 are comparable to the literature range presented in paragraph 1 for both dry and wet conditions. Thus, as for microhardness, additive manufacturing does not seem to affect nor deteriorate the tribological behaviour of the couples of materials. Fig. 9 summarises the main tribological parameters for "dry" tribological tests and evidences similar logarithmic trends for alumina, ZTA10 and ZTA20 wear volume and a different linear growth for zirconia. This means that volume loss reached a plateau for the first three samples, and after a certain sliding distance, there would be no more abrasion. This does not happen for zirconia during the tested sliding distance. Microstructures before and after the tribological test were analysed to understand the different behaviours. By observing Fig. 10, no particular structural changes were detected for ZTA10 and ZTA20 on the tribology tracks after the test. The grains presented the same size, shape and distribution. The effect of the tribological test could be comparable to a polishing treatment: the surface was smoothened, but there was no evidence of continuous tribofilm formation. A third-body was only noticed in the few superficial cavities, as shown in Fig. 12. The case of 3YZ was slightly different: a plastic deformation was detected on the worn zone (Fig. 10). This is common for zirconia subjected to friction and high stress [61,62]. Further analyses should be implemented to evaluate the presence of the tetragonal-to-monoclinic phase transformation that can be induced by low thermal degradation of zirconia. This phenomenon, well known in literature [63–65], is emphasised in the presence of humid environments and affects the mechanical resistance and toughness. Thus, it could be related to the high wear of 3YZ samples. The alumina worn surface had a significantly different morphology and the presence of some holes on the worn surface helped to detect a tribofilm. The surface cross polishing combined with SEM analysis allowed for confirmation of the presence of the tribofilm (Fig. 11) with an approximate thickness of around 1–2 µm. This phenomenon, also called tribo-sintering, has already been reported in the literature [57,66] and only happens under certain humidity and surface finish (open porosity and roughness). It consists of the accumulation of nano-debris that fill holes generated by surface irregularity and are compacted by the counterpart fractioning and pressing [67,68].

The formation of a tribofilm could be very interesting because, in the case of porous or highly irregular surfaces -common characteristics for additive manufactured parts in general- tribofilms offer protection, as a low shear renewable interface, and the resulting tribological properties are similar to more dense microstructures like ZTA. However, the degradation of the tribofilm, if the latter presents a low adherence to the substrate or a fragile nature, could also lead to debris formation. Moreover it is known that, for similar materials (as alumina and ZTA compositions), high density and fine grain size can improve wear resistance (mainly due to their direct relation with hardness) [69,70]. This could explain the lower wear coefficients of ZTA10 and ZTA20. These materials, however, are probably the best choice for their optimal mechanical wear resistance and high hardness. Furthermore, the limited evidence of a third body formation as a tribofilm for these systems, reduces the risk of nano-sized debris dispersion, that could be dangerous in medical applications as bone implants [71–73].

5. Conclusions

This study showed that additive manufacturing by DLP technology allows the obtention of final sintered ceramics that present properties such as microhardness and wettability as well as dry and lubricated tribological behaviour comparable with materials processed by conventional methods. Printing orientation along the xy-plane or xz-plane did not significantly impact microhardness, wettability, and microporosity. However, the staircase effect was observed on the ball curved surfaces, where visible layers increased the surface roughness, especially in the case of ZTA20 and 3YZ zirconia. In general, considering the mechanical, surface properties and tribological behaviours, zirconia toughened alumina systems offered the best compromise and would be the most suitable materials for the envisaged orthopaedic applications. While yttria-stabilised zirconia system presented a high wear rate and friction coefficient for this purpose, alumina system showed acceptable and stable coefficient values. The formation of a tribo-sintered film, in case of high adherence to the substrate and good mechanical properties, could open more possibilities for the AM of joint implants or even for completely different tribological applications such as in aerospace and

automotive fields (bearing tools, combustion engine components, gas turbines).

Funding

This project has received funding from the European Union's Horizon 2020 research and innovation programme under the Marie Skłodowska-Curie grant agreement No 764935.

Declaration of interests

The authors declare that they have no known competing financial interests or personal relationships that could have appeared to influence the work reported in this paper.

References

[1] N. Travitzky, A. Bonet, B. Dermeik, T. Fey, I. Filbert-Demut, L. Schlier, T. Schlordt, P. Greil, Additive manufacturing of ceramic-based materials, Adv. Eng. Mater. 16 (2014) 729–754, https://doi.org/10.1002/adem.201400097.
[2] A. Zocca, P. Colombo, C.M. Gomes, J. Günster, Additive manufacturing of ceramics: issues, potentialities, and opportunities, J. Am. Ceram. Soc. 98 (2015) 1983–2001, https://doi.org/10.1111/jace.13700.
[3] F. Chen, Y.-R. Wu, J.-M. Wu, H. Zhu, S. Chen, S.-B. Hua, Z.-X. He, C.-Y. Liu, J. Xiao, Y.-S. Shi, Preparation and characterization of ZrO2-Al2O3 bioceramics by stereolithography technology for dental restorations, Addit. Manuf. 44 (2021), 102055, https://doi.org/10.1016/j.addma.2021.102055.
[4] J.W. Choi, R. Wicker, S.H. Lee, K.H. Choi, C.S. Ha, I. Chung, Fabrication of 3D biocompatible/biodegradable micro-scaffolds using dynamic mask projection microstereolithography, J. Mater. Process. Technol. 209 (2009) 5494–5503, https://doi.org/10.1016/j.jmatprotec.2009.05.004.
[5] O. Santoliquido, P. Colombo, A. Ortona, Additive Manufacturing of ceramic components by Digital Light Processing: a comparison between the "bottom-up" and the "top-down" approaches, J. Eur. Ceram. Soc. 39 (2019) 2140–2148, https://doi.org/10.1016/j.jeurceramsoc.2019.01.044.
[6] F. Liravi, S. Das, C. Zhou, Separation force analysis and prediction based on cohesive element model for constrained-surface Stereolithography processes, CAD Comput. Aided Des. 69 (2015) 134–142, https://doi.org/10.1016/j.cad.2015.05.002.
[7] X. Song, Y. Chen, T.W. Lee, S. Wu, L. Cheng, Ceramic fabrication using Mask-Image-Projection-based Stereolithography integrated with tape-casting, J. Manuf. Process. 20 (2015) 456–464, https://doi.org/10.1016/j.jmapro.2015.06.022.
[8] Z. Chen, Z. Li, J. Li, C. Liu, C. Lao, Y. Fu, C. Liu, Y. Li, P. Wang, Y. He, 3D printing of ceramics: a review, J. Eur. Ceram. Soc. 39 (2019) 661–687, https://doi.org/10.1016/j.jeurceramsoc.2018.11.013.
[9] S. Baumgartner, M. Pfaffinger, B. Busetti, J. Stampfl, Comparison of dynamic mask- and vector-based ceramic stereolithography, Proc. 41st Int. Conf. Adv. Ceram. Compos. Ceram. Eng. Sci. Proc. 38 (2017) 165–173.
[10] S. Waheed, J.M. Cabot, N.P. Macdonald, T. Lewis, R.M. Guijt, B. Paull, M. C. Breadmore, 3D printed microfluidic devices: enablers and barriers, R. Soc. Chem. 16 (2016) 1993–2013, https://doi.org/10.1039/c6lc00284f.
[11] M. Afshar, A.P. Anaraki, H. Montazerian, J. Kadkhodapour, Additive manufacturing and mechanical characterization of graded porosity scaffolds designed based on triply periodic minimal surface architectures, J. Mech. Behav. Biomed. Mater. 62 (2016) 481–494, https://doi.org/10.1016/j.jmbbm.2016.05.027.
[12] W. Van Grunsven, E. Hernandez-nava, G.C. Reilly, R. Goodall, Fabrication and mechanical characterisation of titanium lattices with graded porosity, Metals 4 (2014) 401–409, https://doi.org/10.3390/met4030401.
[13] M. Vlasea, Y. Shanjani, A. Basalah, E. Toyserkani, Additive manufacturing of scaffolds for tissue engineering of bone and cartilage, Int. J. Adv. Manuf. Syst. 13 (2011) 124–141.
[14] W.W. Thein-Han, R.D.K. Misra, Biomimetic chitosan–nanohydroxyapatite composite scaffolds for bone tissue engineering, Acta Biomater. 5 (2009) 1182–1197, https://doi.org/10.1016/j.actbio.2008.11.025.
[15] S. Eqtesadi, A. Motealleh, P. Miranda, A. Pajares, A. Lemos, J.M.F. Ferreira, Robocasting of 45S5 bioactive glass scaffolds for bone tissue engineering, J. Eur. Ceram. Soc. 34 (2014) 107–118, https://doi.org/10.1016/j.jeurceramsoc.2013.08.003.
[16] H.P. Jost, Tribology - origin and future, Wear 136 (1990) 1–17, https://doi.org/10.1016/0043-1648(90)90068-L.
[17] S. Affatato, L. Grillini, Topography in bio-tribocorrosion, in: Bio-Tribocorrosion Biomater. Med. Implant, Woodhead Publishing Limited, 2013, pp. 1–21, https://doi.org/10.1533/9780857098603.1.
[18] J.G. Lenard, Tribology, in: Prim. Flat Roll, second ed., 2014, pp. 193–266, https://doi.org/10.1016/B978-0-08-099418-5.00009-3.
[19] Z. Jin, J. Fisher, Tribology in joint replacement, in: Jt. Replace. Technol, 2008, pp. 31–55, https://doi.org/10.1533/9781845694807.1.31.
[20] B.F. Morrey, D.J. Berry, in: Joint Replacement Arthroplasty, fourth ed., Lippincott Williams & Wilkins, 2011.
[21] B.S. Bal, J. Garino, M. Ries, M.N. Rahaman, A review of ceramic bearing materials in total joint arthroplasty, HIP Int. 17 (2007) 21–30, https://doi.org/10.5301/HIP.2008.3092.
[22] S.C. Tung, M.L. McMillan, E.P. Becker, S.E. Schwartz, Handbook of Lubrication and Tribology, 2006, https://doi.org/10.1201/9781420003840.sec1 vol. I.
[23] A. Ravikiran, S. Jahanmir, Effect of contact pressure and load on wear of alumina, Wear 251 (2001) 980–984.
[24] H. Heshmat, S. Jahanmir, Tribological behavior of ceramics at high sliding speeds in steam, Tribol. Lett. 17 (2004).
[25] P.J. Blau, Four Great Challenges Confronting Our Understanding and Modeling of Sliding Friction, Elsevier Masson SAS, 1998, https://doi.org/10.1016/s0167-8922(98)80067-9.
[26] M. Guezmil, W. Bensalah, S. Mezlini, Tribological behavior of UHMWPE against TiAl6V4 and CoCr28Mo alloys under dry and lubricated conditions, J. Mech. Behav. Biomed. Mater. 63 (2016) 375–385, https://doi.org/10.1016/j.jmbbm.2016.07.002.
[27] D. Baykal, R.S. Siskey, H. Haider, V. Saikko, T. Ahlroos, S.M. Kurtz, Advances in tribological testing of artificial joint biomaterials using multidirectional pin-on-disk testers, J. Mech. Behav. Biomed. Mater. 31 (2014) 117–134, https://doi.org/10.1016/j.jmbbm.2013.05.020.
[28] C. Kaddick, M.A. Wimmer, Hip simulator wear testing according to the newly introduced standard ISO 14242, Proc. Inst. Mech. Eng. 215 (2001) 429–442, https://doi.org/10.1016/s0021-9290(04)00168-x.
[29] Z. Pawlak, A.D. Petelska, W. Urbaniak, K.Q. Yusuf, A. Oloyede, Relationship between wettability and lubrication characteristics of the surfaces of contacting phospholipid-based membranes, Cell Biochem. Biophys. 65 (2013) 335–345, https://doi.org/10.1007/s12013-012-9437-z.
[30] S. Ghosh, D. Choudhury, T. Roy, A. Moradi, H.H. Masjuki, B. Pingguan-Murphy, Tribological performance of the biological components of synovial fluid in artificial joint implants, Sci. Technol. Adv. Mater. 16 (2015), 45002, https://doi.org/10.1088/1468-6996/16/4/045002.
[31] M.P. Gispert, A.P. Serro, R. Colaço, B. Saramago, Friction and wear mechanisms in hip prosthesis: comparison of joint materials behaviour in several lubricants, Wear 260 (2006) 149–158, https://doi.org/10.1016/j.wear.2004.12.040.
[32] S.M. Hafis, R.N. Farahana, M.J.M. Ridzuan, M.T.N. Adlina, Optimal coefficient of friction on artificial knee joint contact surfaces, Adv. Mater. Res. 716 (2013) 565–568. https://doi.org/10.4028/www.scientific.net/AMR.716.565.
[33] M.J. Nine, D. Choudhury, A.C. Hee, R. Mootanah, N.A.A. Osman, Wear debris characterization and corresponding biological response: artificial hip and knee joints, Materials 7 (2014) 980–1016, https://doi.org/10.3390/ma7020980.
[34] K.G. Plumlee, C.J. Schwartz, Surface layer plastic deformation as a mechanism for UHMWPE wear, and its role in debris size, Wear 301 (2013) 257–263, https://doi.org/10.1016/j.wear.2012.11.081.
[35] H. Li, M. Ramezani, M. Li, C. Ma, J. Wang, Effect of process parameters on tribological performance of 316L stainless steel parts fabricated by selective laser melting, Manuf. Lett. 16 (2018) 36–39, https://doi.org/10.1016/j.mfglet.2018.04.003.
[36] O.A. Mohamed, S.H. Masood, J.L. Bhowmik, A.E. Somers, Investigation on the tribological behavior and wear mechanism of parts processed by fused deposition additive manufacturing process, J. Manuf. Process. 29 (2017) 149–159, https://doi.org/10.1016/j.jmapro.2017.07.019.
[37] S. Perepelkina, P. Kovalenko, R. Pechenko, K. Makhmudova, Investigation of friction coefficient of various polymers used in rapid prototyping technologies with different settings of 3D printing, Tribol. Ind. 39 (2017) 519–526, https://doi.org/10.24874/ti.2017.39.04.11.
[38] M.W. Gonçalves, G.V. Salmoria, C.H. Ahrens, A.S. Pouzada, Study of tribological properties of moulds obtained by stereolithography, Virtual Phys. Prototyp. 2 (2007) 29–36, https://doi.org/10.1080/17452750701295765.
[39] J. Schiltz, A. Rosenberger, T. Render, B.A. Gatrell, H. Qu, C. Steiner, P. McGinn, S. Schmid, Wear of structural oxide ceramics produced through additive manufacturing, Procedia Manuf 34 (2019) 780–788, https://doi.org/10.1016/j.promfg.2019.06.206.
[40] J. Schiltz, T. Render, B.A. Gatrell, H. Qu, C. Steiner, P. McGinn, S. Schmid, Wear behavior of additive manufactured zirconia, Procedia Manuf 48 (2020) 821–827, https://doi.org/10.1016/j.promfg.2020.05.119.
[41] J.F. Archard, W. Hirst, The wear of metals under unlubricated conditions, Proc. R. Soc. London. Ser. A. Math. Phys. Sci. 236 (1956) 397–410, https://doi.org/10.1098/rspa.1956.0144.
[42] H.J. Hu, W.J. Huang, Studies on wears of ultrafine-grained ceramic tool and common ceramic tool during hard turning using Archard wear model, Int. J. Adv. Manuf. Technol. 69 (2013) 31–39, https://doi.org/10.1007/s00170-013-5003-0.
[43] O. Borrero-Lopez, F. Guiberteau, Y. Zhang, B.R. Lawn, Wear of ceramic-based dental materials, J. Mech. Behav. Biomed. Mater. 92 (2019) 144–151, https://doi.org/10.1016/j.jmbbm.2019.01.009.
[44] E. Salihoglu-Yener, M. Ozcan, E. Kazazoglu, A comparative study of biaxial flexural strength and Vickers microhardness of different zirconia materials: effect of glazing and thermal cycling, Brazilian Dent. Sci. 18 (2015) 19, https://doi.org/10.14295/bds.2015.v18i2.1109.
[45] T.J. Lucas, N.C. Lawson, G.M. Janowski, J.O. Burgess, Effect of grain size on the monoclinic transformation, hardness, roughness, and modulus of aged partially stabilized zirconia, Dent. Mater. 31 (2015) 1487–1492, https://doi.org/10.1016/j.dental.2015.09.014.
[46] M.A. Gafur, M.S.R. Sarker, M.Z. Alam, M.R. Qadir, Effect of 3 mol% yttria stabilized zirconia addition on structural and mechanical properties of alumina-zirconia composites, Mater. Sci. Appl. (2017) 584–602, https://doi.org/10.4236/msa.2017.87041, 08.

[47] J.W. An, D.H. You, D.S. Lim, Tribological properties of hot-pressed alumina-CNT composites, Wear 255 (2003) 677–681, https://doi.org/10.1016/S0043-1648(03)00216-3.
[48] A. Salehi, S. Tsai, V. Pawar, J. Sprague, G. Hunter, S.K. Varma, F. Namavar, Wettability analysis of orthopaedic materials using optical contact angle methods, Key Eng. Mater. (2006) 1199–1202. https://doi.org/10.4028/www.scientific.net/kem.309-311.1199, 309–311.
[49] K.J. Kubiak, M.C.T. Wilson, T.G. Mathia, P. Carval, Wettability versus roughness of engineering surfaces, Wear 271 (2011) 523–528, https://doi.org/10.1016/j.wear.2010.03.029.
[50] Y.J. Wang, Z.M. Liu, Micro-pore structure and mechanical properties of high temperature self-lubricating biomimetic TiC/FeCrWMoV cermets, Mater. Sci. Forum (2007) 2273–2278. https://doi.org/10.4028/www.scientific.net/msf.546-549.2273, 546–549.
[51] O. Borrero-Lopez, A. Pajares, P.J. Constantino, B.R. Lawn, A model for predicting wear rates in tooth enamel, J. Mech. Behav. Biomed. Mater. 37 (2014) 226–234, https://doi.org/10.1016/j.jmbbm.2014.05.023.
[52] P. Andersson, A. Blomberg, Alumina in unlubricated sliding point, line and plane contacts, Wear 170 (1993) 191–198, https://doi.org/10.1016/0043-1648(93)90240-M.
[53] N.R. Tedesco, E.M.J.A. Pallone, R. Tomasi, Effects of the pin-on-disc parameters on the wear of alumina, Adv. Sci. Technol. 65 (2010) 39–44. https://doi.org/10.4028/www.scientific.net/ast.65.39.
[54] P. Andersson, K. Holmberg, Limitations on the use of ceramics in unlubricated sliding applications due to transfer layer formation, Wear 175 (1994) 1–8, https://doi.org/10.1016/0043-1648(94)90162-7.
[55] G. Willmann, H.J. Früh, H.G. Pfaff, Wear characteristics of sliding pairs of zirconia, Y-TZP) for hip endoprostheses 17 (1996) 2157–2162.
[56] H.S. Ahn, J.Y. Kim, D.S. Lim, Tribological behaviour of plasma-sprayed zirconia coatings, Wear 203–204 (1997) 77–87, https://doi.org/10.1016/S0043-1648(96)07395-4.
[57] H. Chen, Y. Zhang, C. Ding, Tribological properties of nanostructured zirconia coatings deposited by plasma spraying, Wear 253 (2002) 885–893, https://doi.org/10.1016/S0043-1648(02)00221-1.
[58] J. Chevalier, What future for zirconia as a biomaterial? Biomaterials 27 (2006) 535–543, https://doi.org/10.1016/j.biomaterials.2005.07.034.
[59] J. Chevalier, L. Gremillard, Ceramics for medical applications: a picture for the next 20 years, J. Eur. Ceram. Soc. 29 (2009) 1245–1255, https://doi.org/10.1016/j.jeurceramsoc.2008.08.025.
[60] V. Lughi, V. Sergo, Low temperature degradation -aging- of zirconia: a critical review of the relevant aspects in dentistry, Dent. Mater. 26 (2010) 807–820, https://doi.org/10.1016/j.dental.2010.04.006.
[61] J. Olofsson, U. Bexell, S. Jacobson, Tribofilm formation of lightly loaded self mated alumina contacts, Wear 289 (2012) 39–45, https://doi.org/10.1016/j.wear.2012.03.007.
[62] K. Adachi, K. Kato, Formation of smooth wear surfaces on alumina ceramics by embedding and tribo-sintering of fine wear particles, Wear 245 (2000) 84–91, https://doi.org/10.1016/S0043-1648(00)00468-3.
[63] H. Kato, K. Komai, Tribofilm formation and mild wear by tribo-sintering of nanometer-sized oxide particles on rubbing steel surfaces, Wear 262 (2007) 36–41, https://doi.org/10.1016/j.wear.2006.03.046.
[64] A. Leyland, A. Matthews, On the significance of the H/E ratio in wear control: a nanocomposite coating approach to optimised tribological behaviour, Wear 246 (2000) 1–11.
[65] W. Zhai, L. Bai, R. Zhou, X. Fan, G. Kang, Y. Liu, Recent progress on wear-resistant materials: designs, properties, and applications, Adv. Sci. (2021) 1–29, https://doi.org/10.1002/advs.202003739.
[66] J.L. Tipper, P.J. Firkins, A.A. Besong, P.S.M. Barbour, J. Nevelos, M.H. Stone, E. Ingham, J. Fisher, Characterisation of wear debris from UHMWPE on zirconia ceramic, metal-on-metal and alumina ceramic-on-ceramic hip prostheses generated in a physiological anatomical hip joint simulator, Wear 250 (2001) 120–128.
[67] M.A. Germain, A. Hatton, S. Williams, J.B. Matthews, M.H. Stone, J. Fisher, E. Ingham, Comparison of the cytotoxicity of clinically relevant cobalt – chromium and alumina ceramic wear particles in vitro, Biomaterials 24 (2003) 469–479.
[68] J. Denape, Third body concept and wear particle behavior in dry friction sliding conditions, Key Eng. Mater. 640 (2015) 1–12. https://doi.org/10.4028/www.scientific.net/KEM.640.1.